The $^{31}P\{^1H\}$ NMR spectra of the nitrile complexes appear as sharp singlets at 129.6–138.8 ppm, indicating the presence of four equivalent phosphorus nuclei, as expected for the trans arrangement of the carbonyl and nitrile ligands in the complexes.

Acetonitrile reacts with the diazene complexes to give yellow-white products whose elemental analyses and conductivity data agree with those of the $[Fe(CO)(CH_3CN)L_4]^{2+}$ derivative. Although the infrared spectra of both solid and solution samples do not show any absorption in the CN stretching region,[41] the ^1H NMR spectra in hexadeuterioacetone or CD_2Cl_2, besides the phosphite and BPh_4 signals, show a broad resonance near δ 2.20 attributable to the methyl protons of the acetonitrile ligand. Furthermore, in CD_3CN solvent ligand exchange is observed with the appearance, after 10–20 min, of the singlet at δ 1.96 of the free acetonitrile ligand, thus confirming the proposed formulation for the compound.

Adiponitrile also reacts with the starting Fe(II) complexes but only gives the monosubstituted dication $[Fe(CO)\{NC(CH_2)_4CN\}L_4]^{2+}$ at all ligand:complex ratios. The infrared spectrum shows two ν(CN) bands at 2296 and 2248 cm^{-1}, attributable to the coordinated and free CN group, respectively. An increase of 48 cm^{-1} as compared to the free ligand value is observed, like that found for the aryl cyanide complexes, and suggests similar bonding properties. Finally, the $^{31}P\{^1H\}$ NMR spectra also show that the alkyl cyanide derivatives have the carbonyl and RCN ligands in the trans position.

(41) The low intensity or even absence of ν(CN) in acetonitrile complexes is a feature that has already been observed: Rouschias, G.; Wilkinson, G. *J. Chem. Soc. A* **1967**, 993.

Acknowledgment. The financial support of the MPI and CNR, Rome, is gratefully acknowledged. We thank Daniela Baldan for technical assistance.

Registry No. *trans*-$[FeH(CO)\{P(OMe)_3\}_4]BPh_4$, 100112-66-1; *trans*-$[FeH(CO)\{P(OEt)_3\}_4]BPh_4$, 95738-79-7; *trans*-$[FeH(CO)\{PhP(OEt)_2\}_4]BPh_4$, 100112-68-3; *trans*-$[FeH(CO)\{P(OEt)_3\}_4]Br$, 100112-69-4; $[Fe(4\text{-}CH_3C_6H_4N{=}NH)(CO)\{P(OEt)_3\}_4](BPh_4)_2$, 95738-81-1; $[Fe(4\text{-}ClC_6H_4N{=}NH)(CO)\{P(OEt)_3\}_4](BPh_4)_2$, 100112-71-8; $[Fe(CO)\{(CH_3)_2CO\}\{P(OMe)_3\}_4](BPh_4)_2$, 100112-73-0; $[Fe(CO)\{(CH_3)_2CO\}\{P(OEt)_3\}_4](BPh_4)_2$, 95738-89-9; $[Fe(CO)\{(CH_3)(C_6H_5)CO\}\{P(OEt)_3\}_4](BPh_4)_2$, 100112-75-2; $[Fe(CO)\{(CD_3)_2CO\}\{P(OEt)_3\}_4](BPh_4)_2$, 100112-77-4; $[Fe(CO)\{(CH_3)(C_2H_5)CO\}\{P(OEt)_3\}_4](BPh_4)_2$, 100112-79-6; $[Fe(CO)\{(C_5H_{10})CO\}\{P(OEt)_3\}_4](BPh_4)_2$, 100112-81-0; $[Fe(H_2O)(CO)\{P(OEt)_3\}_4](BPh_4)_2$, 100112-83-2; $[FeCl(CO)\{P(OMe)_3\}_4]BPh_4$, 100112-85-4; $[FeCl(CO)\{P(OEt)_3\}_4]BPh_4$, 100112-87-6; $[FeCl(CO)\{PhP(OEt)_2\}]BPh_4$, 100112-89-8; *cis*-$[FeBr(CO)\{P(OEt)_3\}_4]Br$, 100112-90-1; $[Fe(CO)(4\text{-}CH_3C_6H_4NC)\{P(OEt)_3\}_4]^{2+}$, 100227-13-2; $[Fe(CO)(C_6H_5NC)\{P(OEt)_3\}_4]^{2+}$, 100112-91-2; $[Fe(CO)(4\text{-}CH_3OC_6H_4NC)\{P(OEt)_3\}_4]^{2+}$, 100112-92-3; $[Fe(CO)(4\text{-}NO_2C_6H_4NC)\{P(OEt)_3\}_4]^{2+}$, 100112-93-4; $[Fe(CO)\{2,6\text{-}(CH_3)_2C_6H_3NC\}\{P(OEt)_3\}_4]^{2+}$, 100112-94-5; $[Fe(CO)(4\text{-}CH_3C_6H_4CN)\{P(OMe)_3\}_4]^{2+}$, 100112-95-6; $[Fe(CO)(4\text{-}CH_3C_6H_4CN)\{P(OEt)_3\}_4]^{2+}$, 100227-14-3; $[Fe(CO)(C_6H_5CN)\{P(OEt)_3\}_4]^{2+}$, 100112-96-7; $[Fe(CO)(2\text{-}CH_3C_6H_4CN)\{P(OEt)_3\}_4]^{2+}$, 100112-97-8; $[Fe(CO)(CH_3CN)\{P(OEt)_3\}_4]^{2+}$, 100112-98-9; $[Fe(CO)\{NC(CH_2)_4CN\}\{P(OEt)_3\}_4]^{2+}$, 100112-99-0; $[Fe(CO)_2\{P(OEt)_3\}_4]^{2+}$, 100227-15-4; $[Fe(CO)(4\text{-}CH_3C_6H_4NC)\{P(OMe)_3\}_4]^{2+}$, 100113-00-6; $4\text{-}CH_3C_6H_4N_2^+BF_4^-$, 459-44-9; $4\text{-}ClC_6H_4N_2^+BF_4^-$, 673-41-6; Zn, 7440-66-6.

Supplementary Material Available: Tables of structure factors and thermal parameters and a full list of bond lengths, bond angles, and torsion angles (20 pages). Ordering information is given on any current masthead page.

Contribution from the Department of Chemistry,
Massachusetts Institute of Technology, Cambridge, Massachusetts 02139

Synthesis, Structure, and ^{195}Pt NMR Solution Studies of a Reactive Binuclear Platinum(III) Complex: $[Pt_2(en)_2(C_5H_4NO)_2(NO_2)(NO_3)](NO_3)_2\cdot 0.5H_2O$

Thomas V. O'Halloran, Michael M. Roberts, and Stephen J. Lippard*

Received September 25, 1985

Oxidation of the α-pyridonate- (C_5H_4NO-) bridged diplatinum(II) complex $[Pt_2(en)_2(C_5H_4NO)_2]^{2+}$ (**2**), where en = ethylenediamine, in nitric acid leads to the formation of a metal–metal-bonded diplatinum(III) complex, $[Pt_2(en)_2(C_5H_4NO)_2(NO_2)(NO_3)]^{2+}$ (**1**). In the structure of **1**, two (ethylenediamine)diplatinum(III) units are linked by a metal–metal single bond and two α-pyridonate ligands bridging in a head-to-head fashion. The 2.6382 (6) Å Pt–Pt bond axis is capped by nitrite, Pt–N = 2.109 (1) Å, and nitrate, Pt–O = 2.307 (9) Å, ligands. These Pt–axial ligand distances nicely illustrate a structural trans influence mediated by the metal–metal bond. The coordinated nitrite group is disordered over two positions about the Pt–N axis and is bonded to the platinum atom having two N- and two O-donor ligands. As shown by ^{195}Pt NMR spectroscopy, **1** has a binuclear, metal–metal-bonded structure in freshly prepared aqueous or dimethylformamide (DMF) solutions. In DMF the platinum resonances occur at +541 (PtN_3O_2) and −1141 (PtN_4O) ppm from $[PtCl_6]^{2-}$, with $J(^{195}Pt\text{–}^{195}Pt)$ = 6850 Hz. Decomposition of **1** to form **2** occurs slowly in solution, as revealed by ^{195}Pt NMR spectroscopy. Reductive elimination of nitrite (NO_2^-) to form the nitronium (NO_2^+) ion is postulated to explain this decomposition, since nitrobenzene or *p*-nitrophenol is generated in aqueous solutions of **1** containing tetraphenylborate or phenol, respectively. The nitrate salt of compound **1**, $[Pt(en)_2(C_5H_4NO)_2(NO_2)(NO_3)](NO_3)_2\cdot 0.5H_2O$, crystallizes in the monoclinic space group $P2_1/c$ with a = 17.934 (1) Å, b = 11.491 (1) Å, c = 13.507 (1) Å, β = 108.84 (1)°, V = 2634 Å^3, Z = 4, ρ_{calcd} = 2.369 g cm^{-3}, and ρ_{obsd} = 2.379 (5) g cm^{-3}. The structure was refined to R = 0.035 using 2686 diffractometer data with $F_o > 4\sigma(F_o)$.

Introduction

Until recently, there were few examples of complexes containing platinum in the +3 oxidation state. Binuclear species comprise the vast majority of structurally characterized platinum(III) complexes and therefore provide the best opportunity to probe the structural properties and chemical reactivity of this oxidation state.[1] Platinum–platinum single-bond formation is a natural consequence of the d^7–d^7 electronic configuration in these binuclear complexes, all of which contain two or more bridging ligands.

Binuclear *cis*-diammineplatinum(III) complexes, bridged by two 1-methyluracilate[2] or two α-pyridonate[3] ligands in either a head-to-head or head-to-tail manner, have been previously described. They can be prepared by chemical or electrochemical oxidation of the corresponding platinum(II) dimers[3] or tetranuclear

(1) For a review see: O'Halloran, T. V.; Lippard, S. J. *Isr. J. Chem.* **1985**, *25*, 130–137.

(2) Lippert, B.; Schöllhorn, H.; Thewalt, U. *Z. Naturforsch., B: Anorg. Chem. Org. Chem.* **1983**, *38B*, 1441–1445.

(3) Hollis, L. S.; Lippard, S. J. *J. Am. Chem. Soc.* **1983**, *105*, 3494–3503.

(4) (a) For a review see: Lippard, S. J. *Science (Washington, D.C.)* **1982**, *218*, 1075–1082. (b) Barton, J. K.; Szalda, D. J.; Rabinowitz, H. N.; Waszczak, J. W.; Lippard, S. J. *J. Am. Chem. Soc.* **1979**, *101*, 1434–1441.

0020-1669/86/1325-0957$01.50/0

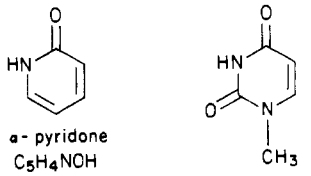

platinum blue ($Pt^{2.25}$) cations, and undergo quasi-reversible two-electron redox reactions.[5] The Pt–Pt bond distances in the head-to-tail complexes vary as a function of the axial ligand in a manner consistent with the established structural trans influence series in mononuclear platinum complexes.[6] Electronic and steric effects associated with the in-plane, or equatorial, ligands also influence the Pt–Pt distance in these $[Pt^{III}]_2$ complexes, but the extent of these interactions has not been investigated.[6b]

In this paper we examine the effects of steric interactions involving the equatorial ligands on the structure, reactivity, and metal–metal bonding for the α-pyridonate-bridged diplatinum(III) cations $[Pt_2(en)_2(C_5H_4NO)_2X_2]^{2+}$ (en = ethylenediamine, X = anion). This system was chosen for study because it already has provided a clear example of the influence of such steric interactions on structure and reactivity for the related binuclear platinum(II) complex $[Pt_2(en)_2(C_5H_4NO)_2]_2(NO_3)_4$.[7,8] The X-ray crystal structure of this binuclear (ethylenediamine)platinum(II) cation revealed pronounced torsional strain and an increased metal–metal distance relative to the *cis*-diammineplatinum(II) analogue. These distortions alter the lability of the platinum(II)–α-pyridonate bonds, resulting in a dramatic enhancement in the rate of linkage isomerization of the bridging α-pyridonate ligand.[8] The distortions observed in the platinum(II) ethylenediamine dimers initially led us to question whether they could be oxidized to metal–metal-bonded $[Pt^{2.25}]_4$ and $[Pt^{III}]_2$ analogues of the *cis*-diammineplatinum(II)/α-pyridone system, since such clusters require much shorter metal–metal distances. A preliminary study suggested that harsh conditions were required to oxidize $[Pt_2(en)_2(C_5H_4NO)_2]^{2+}$ compared to the $[Pt_2(NH_3)_4(C_5H_4NO)_2]^{2+}$ cation, and that the blue $[Pt^{2.25}]_4$ species was observed only as a transient in this reaction.[7] Subsequently, however, we have succeeded in synthesizing and crystallizing the binuclear platinum(III) ethylenediamine complex and report here the structure and chemical reactivity of this interesting species. We have also been able to react this new Pt(III) complex with the known Pt(II) dimer under mild conditions to prepare and characterize the (ethylenediamine)platinum α-pyridone blue, the structure and properties of which are described elsewhere.[9]

Experimental Section

Preparation of Compounds. The starting material, $[Pt_2(en)_2(C_5H_4NO)_2]_2(NO_3)_4$, was obtained as described previously[7] and recrystallized from water. Dimethylformamide (DMF) was distilled over BaO and stored under N_2. All other reagents were used as obtained from commercial sources.

$[Pt_2(en)_2(C_5H_4NO)_2(NO_2)(NO_3)](NO_3)_2\cdot 0.5H_2O$ (1), Head-to-Head Isomer. This compound was obtained by oxidizing $[Pt_2(en)_2(C_5H_4NO)_2](NO_3)_2$ (**2**) with either nitric acid (low yield) or with 1 equiv of $NaNO_2$ in nitric acid (high yield).

Method A: Nitric Acid Oxidation. A slurry of 100 mg (0.12 mmol) of finely ground **2** in 2 mL of 4 M HNO_3 was stirred without heating for 30 min. Four additional 20-mg portions of **2** were added over a 2-h interval. The solution gradually changed color from pale yellow to olive green, and a small fraction of **2** remained undissolved. Upon addition of the final 20-mg portion, the solution changed from green to orange-red and, with continued stirring, most of the starting material dissolved. The solution was filtered and allowed to evaporate in air overnight. A 10-mg crop (5% yield) of well-formed red crystals was collected. Anal. Calcd for $Pt_2C_{14}H_{25}N_{10}O_{13.5}$ (**1**): Pt, 41.5; C, 17.90; H, 2.68; N, 14.91; O, 22.99. Found: Pt, 40.3; C, 17.98; H, 2.73; N, 14.56.

Method B: Sodium Nitrite/Nitric Acid Oxidation. The nitric acid concentration of a freshly prepared aqueous solution of **2** (0.36 g/15 mL) was raised to 3 M by the addition of 3 mL of concentrated nitric acid. Solid $NaNO_2$ (30 mg) was immediately added, and the solution rapidly changed from pale yellow to olive green to orange-red. The mixture was filtered, and crystals began forming in the filtrate after 2 h at room temperature. The solution was allowed to evaporate in air overnight, and 0.27 g (66%) of brick red crystals were collected and washed with 5 mL of H_2O. Typical yields range from 50 to 70%. Anal. Calcd: See above. Found:[10] C, 17.82 (17.89); H, 2.54 (2.71); N, 14.91 (14.82); O, 23.30 (23.40).

Infrared Absorptions. The IR spectra of **1** in Nujol mulls or KBr pellets revealed the following peaks, which were not observed in the spectrum of **2**: 1490 (sh), 1445 (w), 1410 (m), 1290 (s), 1260 (s), 1145 (m), 1010 (m), 805 (m), 635 (w) cm^{-1}.

Nitration Reactions. Nitrobenzene, released when sodium tetraphenylborate was added to an aqueous or nitric acid solution of **1**, was initially identified by its characteristic odor and was subsequently verified by gas chromatography. A 30-μL aliquot of an aqueous solution containing 15 μmol of sodium tetraphenylborate was added to 0.4 mL of a solution containing 3.2 μmol of **1**, and this mixture was extracted with an equal volume of ether. The extract was injected into a Perkin-Elmer Sigma 3 gas chromatograph equipped with a 0.25 in. × 10 ft 4.1% Carbowax/Chromabsorb G column maintained at 180 °C. Three peaks were observed with retention times of 3.2, 3.5, and 6.6 min, respectively. The 3.2-min peak is, at present, unidentified. Co-injection with an authentic sample of nitrobenzene established the 3.5-min peak to be nitrobenzene. Injection of authentic samples of phenol in ether revealed the 6.6-min peak to be phenol. The phenol apparently arises from hydrolysis of tetraphenylborate in a reaction independent of the decomposition of **1**, since ether extracts of 0.5 M HNO_3 or aqueous solutions of tetraphenylborate also revealed the 6.6-min peak characteristic of phenol in their gas chromatograms. The odor of nitrobenzene was also detected when sodium tetraphenylborate was added to a DMF solution of **1**.

Phenol was added to either a neutral or an acidic solution of **1**, under a layer of ether. After 10 min the ether layer was separated and extracted with an aliquot of 1 M NaOH solution, which exhibited a strong absorbance maximum at 400 nm, characteristic of deprotonated 4-nitrophenol.[11] Control reactions using nitrite, nitrate, or complex **2** alone in neutral solutions showed no formation of 4-nitrophenol, judging by the lack of a 400-nm absorption band.

Physical Measurements. Magnetic susceptibility measurements were made on an S.H.E. Corp. SQUID type variable-field susceptometer operating at 10 kG. For typical procedures used in our laboratory see ref 12. ^{195}Pt NMR spectra were acquired on a Bruker WM-250 spectrometer operating at 53.6 MHz. The 90° pulse in a fixed-frequency, 10-mm probe was 25 μs. Infrared measurements were made with a Beckman Acculab 10 instrument.

Collection and Reduction of X-ray Data for $[Pt(en)_2(C_5H_4NO)_2(NO_2)(NO_3)](NO_3)_2\cdot 0.5H_2O$ (1). The orange crystal used in the X-ray diffraction study was a parallelepiped of approximate dimensions 0.05 mm × 0.08 mm × 0.12 mm and was bounded by the faces {001} and {110}. The quality of the crystal, examined by taking open-counter ω scans of several low-angle reflections, was found to be acceptable ($\Delta\bar{\omega}_{1/2}$ = 0.15°). Study on the diffractometer showed the crystal to belong to the monoclinic system, space group $P2_1/c$ (C_{2h}, No. 14).[13] Data collection and reduction proceeded by methods standard in our laboratory,[14] the details of which are presented in Table I.

Structure Solution and Refinement. The positions of the platinum atoms were found by using standard Patterson and direct methods.[15] All

(5) (a) Hollis, L. S.; Lippard, S. J. *J. Am. Chem. Soc.* **1981**, *103*, 6761–6763. (b) Hollis, L. S.; Lippard, S. J. *Inorg. Chem.* **1983**, *22*, 2605–2614.
(6) (a) Hollis, L. S.; Lippard, S. J. *Inorg. Chem.* **1982**, *21*, 2116–2117. (b) Hollis, L. S.; Roberts, M. M.; Lippard, S. J. *Inorg. Chem.* **1983**, *22*, 3637–3644. (c) See also: Alexander, K. A.; Bryan, S. A.; Fronczek, F. R.; Fultz, W. C.; Rheingold, A. L.; Roundhill, D. M.; Stein, P.; Watkins, S. F. *Inorg. Chem.* **1985**, *24*, 2803–2808.
(7) Hollis, L. S.; Lippard, S. J. *Inorg. Chem.* **1983**, *22*, 2600–2604.
(8) O'Halloran, T. V.; Lippard, S. J. *J. Am. Chem. Soc.* **1983**, *105*, 3341–3342.
(9) (a) O'Halloran, T. V.; Roberts, M. M.; Lippard, S. J. *J. Am. Chem. Soc.* **1984**, 106, 6427–6428; and manuscript in preparation.
(10) The first number represents analytical results for a ground sample dried in air for 2 days. The numbers in parentheses report results for a portion of the same sample after it was dried in a vacuum desiccator for 24 h. The agreement between these numbers suggests the lattice water was not removed by vacuum desiccation at room temperature.
(11) Roberts, J. D.; Caserio, M. C. "Basic Principles of Organic Chemistry"; Benjamin: Menlo Park, CA, 1977; p 1402.
(12) Armstrong, W. H.; Spool, A.; Papaefthymiou, G. C.; Frankel, R. B.; Lippard, S. J. *J. Am. Chem. Soc.* **1984**, *106*, 3653–3667.
(13) "International Tables for X-ray Crystallography", 3rd ed.; Kynoch Press: Birmingham, England, 1973; Vol. I, p 99.
(14) Silverman, L. D.; Dewan, J. C.; Giandomenico, C. M.; Lippard, S. J. *Inorg. Chem.* **1980**, *19*, 3379–3383.

Table I. Experimental Details of the X-ray Diffraction Study of $[Pt_2(en)_2(C_5H_4NO)_2(NO_2)(NO_3)](NO_3)_2 \cdot 0.5H_2O$ (1)

(A) Crystal Parameters[a] at 25 °C

a = 17.934 (1) Å	space group = $P2_1/c$
b = 11.491 (1) Å	Z = 4
c = 13.507 (1) Å	ρ_{calcd} = 2.369 g cm^{-3}
β = 108.84 (1)°	ρ_{obsd}[b] = 2.379 (5) g cm^{-3}
V = 2634 Å^3	M_r = 939.6

(B) Measurement of Intensity Data[c]

instrument	Enraf-Nonius CAD-4F κ-geometry diffractometer
radiation	Mo Kα ($\lambda_{\alpha 1}$ = 0.709 30 Å, λ_{α} = 0.710 73 Å) graphite monochromatized
stds,[d] measd every 2.5 h of X-ray exposure time	(313), (3̄13), (4̄02)
no. of reflcns collcd (excluding syst abs)	5041 [3° ≤ 2θ ≤ 50° (+h,+k,±l)]

(C) Treatment of Intensity Data[c]

μ, cm^{-1}	107.9
transmissn factor range[e]	0.421–0.605
averaging,[c] R_{av}	0.016
no. of reflcns after averaging	4613
no. of obsd. unique data [$F_o > 4\sigma(F_o)$]	2686

[a] From a least-squares fit of the setting angles of 25 reflections. [b] By suspension in a mixture of $CHBr_3$ and $CHCl_3$ (four determinations). [c] See ref 14 for typical procedures used in our laboratory. [d] Showed only a random statistical fluctuation. [e] Absorption corrections were performed with the Wehe–Busing–Levy ORABS program.

the remaining non-hydrogen atoms were located from successive difference Fourier maps and refined with anisotropic thermal parameters, except for those atoms which have a significant amount of disorder. There are two disordered forms of the coordinated nitrite group, O(41A)–N(41)–O(42B) and O(41B)–N(41)–O(42A), which are related by rotation of the nitrite group through a small angle about the Pt(2)–N(41) vector. These were best treated by setting each form to 0.5 occupancy during refinement. One of the lattice nitrates, N(31)–O(33), was disordered. It was originally refined as two rigid groups of half-occupancy, with the N–O and O···O distances fixed at 1.23 and 2.13 Å, respectively. This model was less satisfactory than the one ultimately employed in which a single rigid group was refined, albeit with large temperature factors. One isolated peak in the difference Fourier map at 1.44 e Å^{-3} was assigned as a lattice water molecule, O(W), of half occupancy. This atom, together with atoms O(41A), O(41B), O(42A), and O(42B) and N(31)–O(33) were refined with isotropic temperature factors. Neutral-atom scattering factors and anomalous dispersion corrections for non-hydrogen atoms were taken from ref 16 and hydrogen atom scattering factors were taken from ref 17. The hydrogen atoms of the ligands were placed at calculated positions [d(C–H, N–H) = 0.95 Å] and constrained to "ride" on the atoms to which they are attached.[15] The hydrogen atoms of the α-pyridonate rings were refined with a common isotropic thermal parameter that converged to U = 0.038 (13) Å^2. The hydrogen atoms of each ethylenediamine group were refined with an independent set of common isotropic thermal parameters that converged at U = 0.047 (14) Å^2 and 0.040 (13) Å^2. No additional hydrogen atoms were located in the lattice.

Full-matrix least-squares refinement of the structure using 331 parameters converged at R_1 = 0.035 and R_2 = 0.040.[18] The function minimized during the refinement was $\sum w(|F_o| - |F_c|)^2$, where w = $0.9813/[\sigma^2(F_o) + 0.000625F_o^2]$. The maximum parameter shift in the final cycle of refinement was 0.4 σ, and the largest peak on the final difference map (≤1.14 e Å^{-3}) was 0.9 Å from atom Pt(2). The largest peak away from the Pt atoms (1.12 e Å^{-3}) was 1.5 Å from atom O(33). The average $w\Delta^2$ for groups of data sectioned according to parity group, $(\sin\theta)/\lambda$, $|F_o|$, $|h|$, $|k|$, or $|l|$ showed good consistency, and the weighting function was found to be acceptable.

The final atomic positional parameters together with their estimated standard deviations are reported in Table II, while interatomic distances and angles are given in Table III. Listings of final observed and calculated structure factors (Table S1) and atomic thermal parameters (Table S2) are available as supplementary material.

Table II. Final Positional Parameters for $[Pt_2(en)_2(C_5H_4NO)_2(NO_2)(NO_3)](NO_3)_2 \cdot 0.5H_2O$ (1)[a]

ATOM	X	Y	Z
PT1	0.70047(3)	0.48670(4)	0.50166(4)
PT2	0.82133(3)	0.41793(5)	0.66147(4)
O1	0.7354(5)	0.4117(8)	0.7271(7)
O2	0.8349(5)	0.5915(8)	0.6803(7)
O11	0.6058(6)	0.5872(9)	0.3733(7)
O12	0.5048(6)	0.5362(11)	0.4148(10)
O13	0.4915(8)	0.6608(17)	0.3011(16)
O21	0.9494(7)	0.4487(13)	0.2876(10)
O22	0.0782(7)	0.0289(10)	0.0844(9)
O23	0.8645(6)	0.3694(11)	0.3518(9)
N31B	0.6777(7)	0.4534(13)	0.1063(10)
O31B	0.6721(7)	0.3512(13)	0.1303(10)
O32B	0.6727(7)	0.5320(13)	0.1656(10)
O33B	0.6927(7)	0.4765(13)	0.0259(10)
O41A	0.8737(17)	0.415(3)	0.886(2)
O41B	0.8965(20)	0.461(3)	0.876(3)
O42A	0.953(2)	0.324(3)	0.834(3)
O42B	0.9683(17)	0.393(3)	0.820(2)
N41	0.9054(8)	0.4083(14)	0.8122(10)
N1	0.7137(7)	0.4008(10)	0.3759(9)
HN1A	0.7682(7)	0.3900(10)	0.3858(9)
HN1B	0.6905(7)	0.4448(10)	0.3140(9)
N5	0.8217(6)	0.2411(10)	0.6477(9)
HN5A	0.7690(6)	0.2143(10)	0.6181(9)
HN5B	0.8446(6)	0.2072(10)	0.7148(9)
N9	0.6724(6)	0.5630(9)	0.6198(8)
N11	0.5326(8)	0.5962(13)	0.3616(11)
N15	0.7766(6)	0.6190(9)	0.5033(8)
N21	0.0880(7)	-0.0458(13)	0.1500(11)
N8	0.9115(6)	0.4096(10)	0.6021(9)
HN8A	0.9545(6)	0.4543(10)	0.6447(9)
HN8B	0.8947(6)	0.4402(10)	0.5330(9)
N4	0.6233(6)	0.3549(9)	0.4974(9)
HN4A	0.5774(6)	0.3858(9)	0.5081(9)
HN4B	0.6474(6)	0.3004(9)	0.5510(9)
C14	0.6903(8)	0.5049(12)	0.7127(10)
C2	0.6739(8)	0.2857(13)	0.3664(12)
HC2A	0.7086(8)	0.2315(13)	0.4117(12)
HC2B	0.6606(8)	0.2591(13)	0.2962(12)
C3	0.6011(8)	0.2955(13)	0.3961(11)
HC3A	0.5800(8)	0.2206(13)	0.4011(11)
HC3B	0.5629(8)	0.3403(13)	0.3452(11)
C6	0.8675(9)	0.2077(12)	0.5773(12)
HC6A	0.8357(9)	0.2143(12)	0.5060(12)
HC6B	0.8852(9)	0.1296(12)	0.5916(12)
C7	0.9373(9)	0.2863(13)	0.5992(13)
HC7A	0.9746(9)	0.2670(13)	0.6650(13)
HC7B	0.9609(9)	0.2778(13)	0.5459(13)
C10	0.6353(8)	0.6651(12)	0.6089(11)
H10	0.6274(8)	0.7089(12)	0.5466(11)
C11	0.6073(8)	0.7090(13)	0.6862(12)
H11	0.5820(8)	0.7827(13)	0.6779(12)
C12	0.6174(8)	0.6465(13)	0.7730(13)
H12	0.5946(8)	0.6723(13)	0.8236(13)
C13	0.6607(9)	0.5434(13)	0.7900(11)
H13	0.6701(9)	0.5006(13)	0.8531(11)
C16	0.7716(8)	0.6783(13)	0.4145(12)
H16	0.7353(8)	0.6527(13)	0.3500(12)
C17	0.8172(9)	0.7752(14)	0.4143(14)
H17	0.8152(9)	0.8142(14)	0.3515(14)
C18	0.8662(10)	0.8124(15)	0.5097(16)
H18	0.8971(10)	0.8804(15)	0.5134(16)
C19	0.8718(9)	0.7552(14)	0.5994(16)
H19	0.9051(9)	0.7830(14)	0.6650(16)
C20	0.8259(7)	0.6524(12)	0.5942(11)
OW	0.497(4)	0.370(5)	0.050(5)

[a] Numbers in parentheses are errors in the last significant digit(s). Atoms are labeled as shown in Figure 1.

Results and Discussion

The structure of the $[Pt_2(en)_2(C_5H_4NO)_2(NO_2)(NO_3)]^{2+}$ cation in **1** consists of two (ethylenediamine)platinum(III) units bridged by two α-pyridonate ligands in a head-to-head arrangement (Figure 1). The axial sites of both platinum atoms are occupied by a donor atom from the capping ligands, and if the metal–metal bond is included, each platinum is six-coordinate. The platinum

(15) All calculations were performed on a DEC VAX-11/780 computer using SHELX-76: Sheldrick, G. M. In "Computing in Crystallography"; Schenk, H., Olthof-Hazekamp, R., Van Konigsveld, H., Bassi, G. C., Eds.; Delft University Press: Delft, The Netherlands, 1978; pp 34–42.

(16) "International Tables for X-ray Crystallography"; Kynoch Press: Birmingham, England, 1974; Vol. IV, pp 99, 149.

(17) Stewart, R. F.; Davidson, E. R.; Simpson, W. T. *J. Chem. Phys.* **1965**, *42*, 3175–3187.

(18) $R_1 = \sum||F_o| - |F_c||/\sum|F_o|$; $R_2 = [\sum w(|F_o| - |F_c|)^2/\sum w|F_o|^2]^{1/2}$.

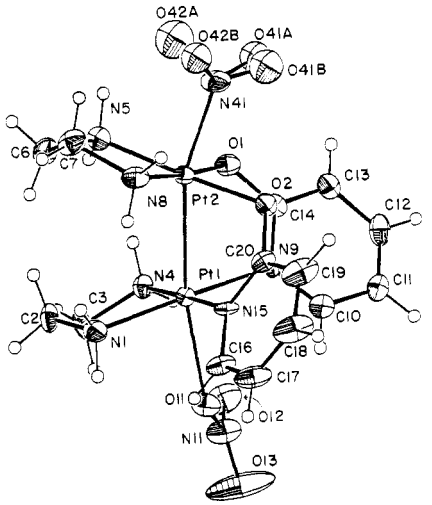

Figure 1. Structure of the α-pyridonate-bridged cation $[Pt_2(en)_2(C_5H_4NO)_2(NO_2)(NO_3)]^{2+}$ (**1**) showing the 40% probability thermal ellipsoids. For clarity, the hydrogen atoms are depicted as spheres with B set to 1 Å^2. The hydrogen atom labels (not shown) are assigned according to the atoms to which they are attached (e.g., H(N4A) is attached to N(4), etc.). Two positions for the disordered nitrite ligand are depicted (see text).

atom (Pt(2)) bound to the exocyclic α-pyridonate oxygen atoms contains a nitrite anion (disordered over two positions) in the axial site while the platinum atom attached to the annular nitrogen atoms (Pt(1)) is coordinated to an oxygen atom (O(11)) of a nitrate anion. The structure may be compared with the only other known binuclear head-to-head α-pyridonate-bridged diplatinum(III) complex, $[Pt_2(NH_3)_4(C_5H_4NO)_2(H_2O)(NO_3)]^{3+}$ (**3**), which contains *cis*-diammine ligands in the equatorial plane and is capped by a water molecule (Pt(2)) and a nitrate anion (Pt(1)).[5] The relative axial ligand affinities in **3** were previously attributed to the different electron density requirements of the two inequivalent platinum atoms. In particular, the preference of the charged nitrate group for Pt(1) was interpreted to imply that the two exocyclic oxygen atoms provide more electron density to Pt(2) than the ring nitrogen atoms provide to Pt(1). In the present structure, however, the more electron-donating nitrite group is coordinated to Pt(2). In the extreme, coordination of nitrite to the platinum atom, Pt(2), having a N_2O_2 donor set in the equatorial plane may result in no axial ligand at all bound to the other platinum in a metal–metal-bonded system.[34] The exocyclic oxygen atoms may render Pt(2) more susceptible than Pt(1) to coordination by a strong nucleophile. Further insight into the axial ligand preferences of bridged binuclear Pt(III) complexes awaits the structural characterization of additional head-to-head compounds having mixed axial ligands and, possibly, calculations of the platinum charge densities in this system.

The Pt–N distances (Table III) for both equatorial ethylenediamine and α-pyridonate nitrogen atoms are within the 2.02–2.06-Å range normally found in related platinum(II) and platinum(III) compounds.[2,5–7] The equatorial Pt–O(pyridonate) bond lengths of **1** are in the usual range (1.99–2.07 Å)[5–7] for $[Pt^{III}]_2$ complexes, and compare favorably with the same bond distances, 2.04 (1) Å, in the related tetranuclear blue complex $[Pt_2(en)_2(C_5H_4NO)_2]_2(NO_3)_5 \cdot H_2O$ (**4**). These Pt–O distances are also an average of 0.035 Å (2σ)[19] shorter than the Pt–O bonds in the $[Pt^{II}]_2$ precursor $[Pt(en)_2(C_5H_4NO)_2]_2(NO_3)_4$ (**2**). The equatorial ligands define a plane with a four-atom rms deviation of 0.027 Å for Pt(1) and 0.11 Å for Pt(2). The two platinum atoms are slightly displaced out of these planes toward one another by 0.041 Å for Pt(1) and 0.065 Å for Pt(2). Displacements of this kind occur to a similar degree[5,6] in other binuclear platinum(III) complexes. The tilt angle (τ) between the adjacent equatorial coordination planes in **1** is 30.7°, and the average torsion angle, ω, or twist about the Pt–Pt vector is 36.2°. Both these values are significantly larger than found in other binuclear platinum(III) complexes. The ranges are typically 20–22° in τ and 23–32° in ω for the $[Pt^{III}]_2$ cations HH-$[Pt_2(NH_3)_4(C_5H_4NO)_2(H_2O)(NO_3)]^{3+}$ (**3**),[5] HT-$[Pt_2(NH_3)_4(C_5H_4NO)_2X_2]^{2+}$ (X = NO_3^- (**5**), Cl^- (**6**), NO_2^- (**7**), Br^- (**8**)),[6a,b] HT-$[Pt_2(NH_3)_4(C_5H_5N_2O_2)(OH_2)(NO_2)]^{3+}$ (**9**)[2], and HT-$[Pt_2(NH_3)_4(C_5H_6N_3O)_2(NO_2)_2]^{3+}$ (**10**).[20]

Table III. Interatomic Distances (Å) and Angles (deg) for $[Pt_2(en)_2(C_5H_4NO)_2(NO_2)(NO_3)](NO_3)_2 \cdot 0.5H_2O$[a]

Coordination Sphere			
Pt(1)-N(1)	2.044(12)	Pt(2)-N(5)	2.041(11)
Pt(1)-N(4)	2.040(11)	Pt(2)-N(8)	2.026(13)
Pt(1)-N(9)	2.022(11)	Pt(2)-O(1)	2.013(11)
Pt(1)-N(15)	2.039(10)	Pt(2)-O(2)	2.015(9)
Pt(1)-O(11)	2.307(9)	Pt(2)-N(41)	2.109(11)
	Pt(1)-Pt(2) 2.6382(6)		
Pt(2)-Pt(1)-O(11)	167.4(3)	Pt(1)-Pt(2)-N(41)	161.4(4)
N(1)-Pt(1)-N(4)	83.0(4)	N(5)-Pt(2)-N(8)	83.7(4)
N(1)-Pt(1)-N(9)	172.3(4)	N(5)-Pt(2)-O(2)	173.3(4)
N(1)-Pt(1)-N(15)	96.4(4)	N(5)-Pt(2)-O(1)	91.7(4)
N(4)-Pt(1)-N(9)	90.3(4)	N(8)-Pt(2)-O(2)	91.0(4)
N(4)-Pt(1)-N(15)	179.0(4)	N(8)-Pt(2)-O(1)	174.6(4)
N(9)-Pt(1)-N(15)	90.3(4)	O(1)-Pt(2)-O(2)	93.3(4)
O(11)-Pt(1)-N(1)	82.7(4)	N(41)-Pt(2)-N(5)	90.8(5)
O(11)-Pt(1)-N(4)	91.3(4)	N(41)-Pt(2)-N(8)	88.1(5)
O(11)-Pt(1)-N(9)	93.8(4)	N(41)-Pt(2)-O(2)	84.9(5)
O(11)-Pt(1)-N(15)	87.9(4)	N(41)-Pt(2)-O(1)	89.0(4)
Ligand Geometry			
O(1)-C(14)	1.317(16)	O(2)-C(20)	1.321(15)
N(9)-C(14)	1.365(15)	N(15)-C(20)	1.317(16)
C(14)-C(13)	1.388(18)	C(20)-C(19)	1.429(19)
C(13)-C(12)	1.395(20)	C(19)-C(18)	1.354(23)
C(12)-C(11)	1.337(19)	C(18)-C(17)	1.372(23)
C(11)-C(10)	1.392(18)	C(17)-C(16)	1.381(19)
C(10)-N(9)	1.333(16)	C(16)-N(15)	1.357(16)
O(1)···N(9)	2.311(13)	O(2)···N(15)	2.301(12)
N(41)-O(41A)	1.30(3)	N(11)-O(11)	1.275(15)
N(41)-O(41B)	1.11(3)	N(11)-O(12)	1.212(15)
N(41)-O(42A)	1.26(4)	N(11)-O(13)	1.171(17)
N(41)-O(42B)	1.11(3)	N(5)-C(6)	1.495(16)
N(1)-C(2)	1.488(17)	C(6)-C(7)	1.494(19)
C(2)-C(3)	1.490(18)	C(7)-N(8)	1.495(17)
C(3)-N(4)	1.464(15)		
Pt(1)-N(9)-C(10)	122.5(9)	C(3)-N(4)-Pt(1)	110.5(8)
Pt(1)-N(9)-C(14)	117.9(8)	Pt(1)-N(15)-C(16)	120.8(9)
Pt(2)-O(1)-C(14)	115.3(7)	Pt(1)-N(15)-C(20)	118.2(8)
C(10)-N(9)-C(14)	119.5(11)	Pt(2)-O(2)-C(20)	116.0(8)
O(1)-C(14)-N(9)	118.9(11)	C(16)-N(15)-C(20)	120.8(11)
O(1)-C(14)-C(13)	120.9(12)	O(2)-C(20)-N(15)	121.4(12)
N(9)-C(14)-C(13)	120.2(13)	O(2)-C(20)-C(19)	119.4(13)
C(14)-C(13)-C(12)	118.3(14)	N(15)-C(20)-C(19)	119.2(13)
C(13)-C(12)-C(11)	120.8(14)	C(20)-C(19)-C(18)	118.8(16)
C(12)-C(11)-C(10)	118.9(14)	C(19)-C(18)-C(17)	122.0(16)
C(11)-C(10)-N(9)	121.6(13)	C(18)-C(17)-C(16)	116.7(15)
Pt(2)-N(41)-O(41A)	112.7(14)	C(17)-C(16)-N(15)	122.4(14)
Pt(2)-N(41)-O(41B)	119.0(19)	Pt(1)-O(11)-N(11)	127.8(9)
Pt(2)-N(41)-O(42A)	119.1(19)	O(11)-N(11)-O(12)	119.0(14)
Pt(2)-N(41)-O(42B)	119.3(17)	O(11)-N(11)-O(13)	121.9(15)
O(41A)-N(41)-O(42B)	127.9(22)	O(12)-N(11)-O(13)	119.2(15)
O(41B)-N(41)-O(42A)	119.6(26)	Pt(2)-N(5)-C(6)	109.4(8)
Pt(1)-N(1)-C(2)	108.6(8)	N(5)-C(6)-C(7)	108.4(12)
N(1)-C(2)-C(3)	110.4(11)	C(6)-C(7)-N(8)	109.4(12)
C(2)-C(3)-N(4)	106.8(11)	C(7)-N(8)-Pt(2)	110.4(8)
Anion Geometry			
N(21)-O(21)	1.236(22)	O(21)-N(21)-O(22)	123.8(15)
N(21)-O(22)	1.205(19)	O(21)-N(21)-O(23)	118.6(14)
N(21)-O(23)	1.300(19)	O(22)-N(21)-O(23)	117.4(15)
Possible Hydrogen Bonds			
O(12)···O(12)'	2.507(28)	O(23)···N(5)	2.904(16)
O(12)···H(N4A)'	2.247(19)	O(23)···O(42A)	2.79(4)
O(12)···N(4)'	3.164(19)	O(31)···H(N5A)	1.949(18)
O(12)···H(N4A)	2.283(15)	O(31)···N(5)	2.823(17)
O(12)···N(4)	2.927(15)	O(31)···H(N4B)	2.018(18)
O(13)···O(W)	3.10(6)	O(31)···N(4)	2.931(17)
O(21)···H(N8A)	2.009(16)	O(31)···O(W)	2.97(6)
O(21)···H(N8)	2.949(16)	O(32)···H(N1B)	2.170(18)
O(22)···H(N8B)'	2.071(18)	O(32)···N(1)	3.087(18)
O(22)···N(8)'	2.925(18)	O(41A)···O(1)	2.71(3)
O(23)···H(N1A)	1.940(18)	O(42A)···O(23)	2.79(4)
O(23)···N(1)	2.848(18)	O(42B)···H(N8A)	2.41(3)
O(23)···H(N5B)	1.974(17)	O(42B)···N(8)	2.80(3)
O(12)···H(N4A)'-N(4)'	161.9(11)	O(23)···H(N5B)'-N(5)'	165.7(13)
O(12)···H(N4A)-N(4)	124.5(12)	O(31)···H(N5A)-N(5)	151.9(13)
O(21)···H(N8A)-N(8)	170.1(14)	O(31)···H(N4B)-N(4)	160.5(11)
O(22)···H(N8B)'-N(8)'	148.8(11)	O(32)···H(N1B)-N(1)	161.7(14)
O(23)···H(1NA)-N(1)	159.3(12)	O(42B)···H(N8A)-N(8)	104.1(13)

[a] See Footnote *a* of Table II. Distances have not been corrected for thermal motion.

(19) The esd is calculated as $\sigma = (\sigma_1^2 + \sigma_2^2)^{1/2}$, where σ_1 and σ_2 are the errors in the bond lengths or angles being compared.

(20) (a) Faggiani, R.; Lippert, B.; Lock, C. J. L.; Speranzini, R. A. *J. Am. Chem. Soc.* **1981**, *103*, 1111–1120. (b) See also ref 6.

Table IV. Comparison of Geometric Properties of Head-to-Head α-Pyridonate-Bridged Platinum Complexes

compd	formal oxidn state	Pt–Pt[a] dist, Å	dihedral angles,[b] deg		ref
			τ	ω	
$[Pt_2(en)_2(C_5H_4NO)_2(NO_2)(NO_3)](NO_3)_2 \cdot 0.5H_2O$ (**1**)	3.0	2.6382 (6)	30.7	36.2	*c*
$[Pt_2(en)_2(C_5H_4NO)_2]_2(NO_3)_5 \cdot H_2O$ (**4**)	2.25	2.8296 (5) 2.9058 (6)	32.1	24.3	9
$[Pt_2(en)_2(C_5H_4NO)_2]_2(NO_3)_4$ (**2**)	2.0	2.992 (1) 3.236 (1)	39.6	24.9	7
$[Pt_2(NH_3)_4(C_5H_4NO)_2(H_2O)(NO_3)](NO_3)_3 \cdot 2H_2O$ (**3**)	3.0	2.540 (1)	20.0	23.2	6a,b
$[Pt_2(NH_3)_4(C_5H_4NO)_2]_2(NO_3)_5 \cdot H_2O$ (**11**)	2.25	2.775 (1) 2.877 (1)	27.4	22.8	4b
$[Pt_2(NH_3)_4(C_5H_4NO)_2]_2(NO_3)_4$ (**12**)	2.0	2.877 (1) 3.129 (1)	30.0	20.3	5

[a] When two distances appear, the first refers to the distance between α-pyridonate-bridged atoms [Pt(1)–Pt(2)] and the second refers to the Pt(2)–Pt(2)′ distances. [b] τ is the tilt angle between adjacent platinum coordination planes in the binuclear unit, and ω is the average torsion angle about the Pt(1)–Pt(2) vector. [c] This work.

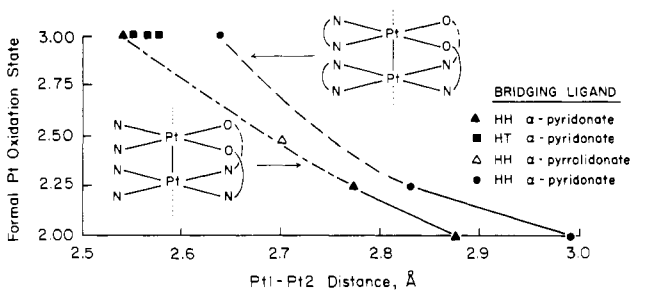

Figure 2. Plot of average platinum oxidation state vs. the bridged platinum–platinum distance (Pt(1)–Pt(2)) for a series of polynuclear *cis*-diammine- and (ethylenediamine)platinum complexes.

The presence of the equatorial ethylenediamine ligand in **1** exerts a greater steric demand than the ammine groups in complexes **3** and **5–10**. As a consequence, the Pt–Pt bond is 0.072 Å (>70σ) longer in **1** compared to the average bond length of **3** and **5–10**. Opening of the twist angle, ω, further minimizes the nonbonded repulsion between the in-plane ligands. The tilt angle, τ, increases with the Pt–Pt distance in a straightforward manner as described in detail elsewhere.[7] The large intradimer Pt–Pt distance of 2.992 (1) Å in **2** corresponds to a tilt angle of 39.6°; both of these values are greater than the analogous parameters in **1**, **3**, and **5–10**.

The bond lengths and angles in both ethylenediamine ligands are within the range found in other ethylenediamine/Pt(II) complexes (C–C–N angles 109–119° and C–C distances 1.29–1.54 Å).[21] In contrast to the ethylenediamine $[Pt^{II}]_2$ precursor **2**,[7] which also has adjacent ethylenediamine rings, there are no disordered ethylene carbon atoms, and both of the torsion angles around these carbon atoms (N(1)–C(2)–C(3)–N(4) = −50.3° and N(5)–C(6)–C(7)–N(8) = −47.6°) approach the ideal ±60° value expected for a gauche conformation about the C–C axes. The two chelate rings assume the same (δ) conformation in **1**, whereas in **2** the rings have opposite conformations. Moreover, the twist angle, ω, opens from 24.9° in **2** to 36.2° in **1**. The latter value is the largest twist observed in the α-pyridonate-bridged binuclear platinum complexes to date and it approaches the 45° angle in a fully staggered conformation of the two equatorial platinum planes. The closest nonbonded contacts between the two equatorial ligand planes are H(C2A)···H(6A) (2.23 Å) and H(N5A)···H(N4B) (2.30 Å).

The interplanar steric repulsions between ethylenediamine ligands influence the metal–metal interaction as shown in Figure 2, where the Pt–Pt distances of the polynuclear ethylenediamine complexes are compared with an analogous series (Table IV) of *cis*-diammine complexes. The Pt(1)–Pt(2) distances are an average of 0.106 ± 0.008 Å longer for ethylenediamine relative to similar *cis*-diammine complexes having the same Pt oxidation state. The constancy of this difference over a 0.4-Å range of Pt(1)–Pt(2) distances results from the ability of these complexes to change the conformation of the two equatorial platinum planes (manifest in the twist angle ω) and to distort the ethylenediamine ring pucker (manifest in the C–C torsion angles), thereby reducing energetically unfavorable nonbonded interactions between hydrogen atoms in adjacent equatorial ethylenediamine ligands.

This torsional strain affects the chemical properties of these complexes. The head-to-head to head-to-tail isomerization of the ethylenediamine $[Pt^{II}]_2$ complex **2** is at least 2 orders of magnitude faster than that of the *cis*-diammine $[Pt^{II}]_2$ complex.[8,33] Here the torsional strain, introduced to minimize the unfavorable nonbonded interactions mentioned above, is probably responsible for the increased lability of what are typically inert Pt–N bonds.[8] This torsional strain is manifest primarily in the tilt angle τ, which is larger than that of any of the previously characterized α-pyridone complexes. The ethylenediamine $[Pt^{II}]_2$ complex is also more difficult to oxidize to the $[Pt^{2.25}]_4$ or $[Pt^{III}]_2$ complexes in comparison to the *cis*-diammine $[Pt^{II}]_2$ analogue, again reflecting the influence of the steric bulk of the equatorial ligands on the chemistry of these compounds.

The bond lengths and angles within the α-pyridonate ligands are similar to those found in related structure determinations and show the usual changes[5-7] from the geometry of the free ligand. The two disordered forms of the coordinate nitrite ligand define planes that are twisted from the plane of atoms Pt(2), O(1), N(41), and N(8) by 8.2° for N(41), O(41A), and O(42B) and by 51.4° for N(41), O(41B), and O(42A). The second form is clearly stabilized by assuming a position with a minimum of nonbonded interligand repulsions. The first form is presumably stabilized by a hydrogen-bonding interaction to a proton on the ethylenediamine nitrogen atom N(8); O(42B)···N(8) = 2.80 (3) Å. This latter interaction is supported by the isotropic thermal parameters for O(41A) (U = 0.076 (8) Å^2) and O(42B) (U = 0.074 (8) Å^2), both significantly smaller than those for O(41B) (U = 0.09 (1) Å^2) and O(42A) (U = 0.12 (1) Å^2). In view of the somewhat high esd's for the nitrite atom positions, the bond distances and angles of each disordered form are equivalent and typical for axial nitrite ligands observed in other diplatinum(III) complexes such as **7**, **9**, and **10**.

A clear example of the structural trans influence mediated by a metal–metal bond can be seen in both the Pt–N(nitrite), 2.109 (11) Å, and Pt–O(nitrate), 2.307 (9) Å, distances in **1**. The former value is significantly shorter than the axial Pt–N(nitrite) distances in **7**, 2.172 (10) and 2.168 (11) Å, while the latter distance is significantly longer than the Pt–O(nitrate) distances in **5**, 2.170 (10) and 2.165 (10) Å, and **3**, 2.193 (7) Å, which has a water molecule capping the other axial position. These differences are due to the ability of the axial groups to weaken a trans ligand bond across the metal–metal bond axis. In both examples, this structural trans influence follows the expected order ($NO_2^- > NO_3^-$). The effect of the trans influence of the axial ligands on the Pt–Pt bond length per se is obfuscated by the previously discussed steric

(21) (a) Faggiani, R.; Lippert, B.; Lock, C. J. L. *Inorg. Chem.* **1980**, *19*, 295–300. (b) Gellert, R. W.; Bau, R. *J. Am. Chem. Soc.* **1975**, *97*, 7379–7380. (c) Neidle, S.; Taylor, G. L.; Robins, A. B. *Acta Crystallogr. Sect. B: Struct. Crystallogr. Cryst. Chem.* **1978**, *B34*, 1838–1841.

Table V. ^{195}Pt Chemical Shifts and $J(^{195}Pt-^{195}Pt)$ Values for Related Binuclear Pt(II) and Pt(III) Complexes

compd	oxidn state	Pt environment[a]	$\delta(^{195}Pt)$[b]	$J(^{195}Pt-^{195}Pt)$, Hz	solvent	temp, °C	ref
$[Pt_2(en)_2(C_5H_4NO)_2(NO_2)(NO_3)](NO_3)_2 \cdot 0.5H_2O$ (**1**)	3.0	N_3O_2	+541[c]	6840	DMF	5	*d*
		N_4O	−1141	6859	DMF		
$[Pt_2(en)_2(C_5H_4NO)_2]_2(NO_3)_4$ (**3**)	2.0	N_2O_2	−1605	<800	H_2O	25	9
		N_4	−2485	<800			
$[Pt_2(PO_4H)_4(Cl)(H_2O)]^{3-}$ (**12**)	3.0	O_5	+1889	5342	H_2O		26
		O_4Cl	+1713	5342			
$[Pt_2(SO_4)_4(Cl)(H_2O)]^{3-}$ (**13**)	3.0	O_5	+1808	3464	H_2O		26
		O_4Cl	+1638	3464			

[a] Ligand atoms in the first coordination sphere—see text. [b] Referenced to K_2PtCl_6 (downfield positive convention). [c] These chemical shifts show little solvent dependence. Both nuclei resonate approximately 35 ppm upfield of these reported values in H_2O (25 °C). The temperature dependence is also small; for example, the N_4O resonance occurs at −1137 ppm at 25 °C in DMF. [d] This work.

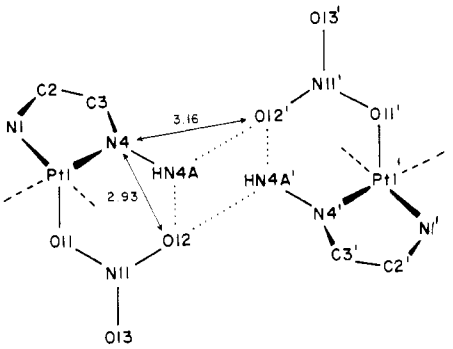

Figure 3. Schematic representation of the bifurcated hydrogen bonds described in the text. A crystallographic inversion center is located midway between the nitrate oxygen atoms O(12) and O(12)′.

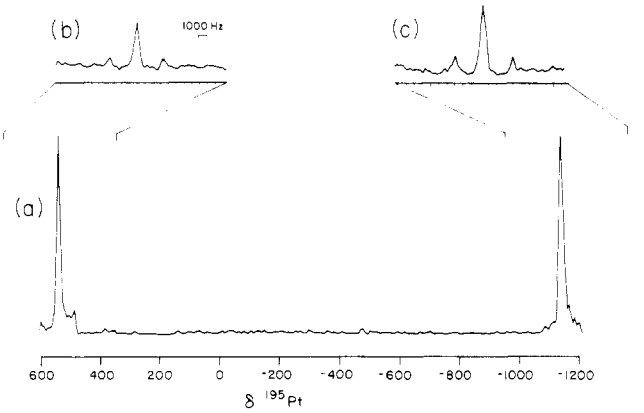

Figure 4. ^{195}Pt NMR spectra of a 16 mM DMF solution of $[Pt_2(en)_2(C_5H_4NO)_2(NO_2)(NO_3)](NO_3)_2 \cdot 0.5H_2O$ (**1**) at 5 °C, acquired on a Bruker WM-250 spectrometer operating at 53.6 MHz: (a) power spectrum of the Fourier transform of a 1K FID accumulated with a 5-μs pulse width, 100-kHz spectral width, and 200K transients; (b and c) normal Fourier transforms of 1K FID's accumulated with 10-μs pulse widths, 42-kHz spectral widths, and 64K transients per spectrum. All FID's were treated with 400-Hz line broadening functions to suppress noise.

interactions of adjacent ethylenediamine ligands, although it is apparent in compounds **5–8**, which contain NH_3 rather than en groups in the equatorial coordination plane.[6a,b]

The geometry of the coordinated nitrate group appears normal, and the bonding angle Pt(1)–O(11)–N(11), 127.8 (9)°, is comparable to the Pt–O–NO_2 angles found in **3**, 124.8 (6)°, and in **5**, 122.6 (10) and 125.8 (10)°. As in structures **3** and **5**, one of the terminal oxygen atoms of the coordinated nitrate in **1** is hydrogen bound to protons on the nitrogen atoms in the equatorial coordination plane. In **1**, atom O(12) is involved in both intramolecular [O(12)···H(N4A) = 2.283 (15) Å, O(12)···H(N4A)–N4 = 124.5 (12)°] and intermolecular [O(12)···H(N4A)′ = 2.247 (19) Å, O(12)···H(N4A)′–N(4)′ = 161.9 (11)°] hydrogen-bonding interactions (Figure 3). The ethylenediamine hydrogen atom (HN4A) is approximately equidistant from the two acceptor atoms (O(12) and O(12)′), and the H···X distances are 0.44 and 0.47 Å shorter than the sum of the van der Waals radii for hydrogen and oxygen (2.72 Å). This interaction therefore fits both of Donohue's criteria for a bifurcated hydrogen bond.[22] Since the two acceptor atoms are related through an inversion center, there are actually two bifurcated hydrogen bonds linking O(12) and O(12)′ and therefore connecting two symmetry related molecules in the unit cell. These two bifurcated hydrogen bonds facilitate the unusually short O(12)···O(12)′ contact of 2.507 (28) Å across the center of inversion. We also considered the possibility that a proton located between O(12) and O(12)′ was present in these crystals, which were grown from a 3 M HNO_3 solution. As discussed below, there is physicochemical evidence against this postulate.

The terminal nitrate oxygen O(13) has an elongated thermal ellipsoid. It may be slightly disordered since it is weakly hydrogen bound with the disordered lattice water present at a 50% occupancy [O(13)···O(W) = 3.10 (6) Å]. The partially occupied lattice water site may also account for the disorder in the lattice nitrate N(31)–O(33) to which it is also hydrogen bound [O(31)···O(W) = 2.97 (6) Å]. The remaining lattice nitrate, N(21), is ordered. All three nitrates play a role in connecting the diplatinum(III) cations by hydrogen bonding to protons on the nitrogen atoms of the ethylenediamine groups.

Chemical and Physical Measurements. Other formulations for **1** were explored and eliminated on the basis of additional physical and chemical evidence. First, we considered the possibility that the axial, nitrogen-bound ligand was not a nitrite disordered over two positions, but rather a bent nitrosyl disordered over four positions. Infrared spectra of **1** in KBr pellets or Nujol mulls, however, revealed no absorptions in the 1500–1900-cm^{-1} range typical of coordinated nitrosyls.[24a] The bond angles and distances are typical of axial nitrites in other binuclear Pt(III) complexes, as detailed above. Comparison of the IR spectra of **1** with the binuclear platinum(II) starting material **2** revealed several new infrared absorptions in the 1000–1500- and 600–800-cm^{-1} range consistent with the presence of M–NO_2 and M–ONO_2 species.[24b] The assignments are not conclusive, however, because of the presence of uncoordinated nitrate ions in the lattice as counterions. Attempts to isolate **1** with other counterions such as ClO_4^-, BF_4^-, or $B(C_6H_5)_4^-$ were unsuccessful. The last reacted with **1** yielding nitrobenzene (vide infra). Finally, density measurements and oxygen–carbon and oxygen–nitrogen ratios obtained from elemental analyses strongly support the formulation of **1** as a nitrite-capped, diplatinum(III) cation with two lattice nitrates and one-half of a water molecule per bimetallic unit.

As mentioned previously, we investigated the possibility that the close approach of the axial nitrates in the crystal lattice was brought about by a lattice proton situated on the inversion center relating O(12) and O(12)′. If this were the case, charge balance

(22) Donohue, J. In "Structural Chemistry and Molecular Bonding"; Rich, A., Davidson, N., Eds.; Freeman: San Francisco, 1968; p 443.
(23) Ardon, M.; Bino, A. *Inorg. Chem.* **1985**, 24, 1343–1347.
(24) (a) Nakamoto, K. "Infrared and Raman Spectra of Inorganic and Coordination Compounds"; Wiley: New York, 1970; pp 200–202. (b) *Ibid.*, p 327.

would require the diplatinum cation to have a nonintegral average oxidation state and, therefore, to be paramagnetic. This possibly was ruled out by ESR and SQUID magnetic susceptibility studies, which reveal crystalline samples of **1** to be diamagnetic. The molar susceptibilities, with diamagnetic corrections calculated from Pascal's constants (see ref 12), were $\chi_M^{cor} = +9.1 \times 10^{-6}$ and -4.6×10^{-6} cgsu at 8 and 300 K, respectively. Aqueous solutions of **1** also show distinct NMR signals in the range expected for diamagnetic Pt(III) complexes (vide infra).

^{195}Pt NMR Studies. The formulation of **1** as a diamagnetic metal–metal bonded $[Pt^{III}]_2$ complex is further corroborated by the results of solution ^{195}Pt NMR studies summarized in Table V. Fresh aqueous or DMF solutions of **1** exhibit two widely separated resonances, downfield of the analogous resonances in the $[Pt^{II}]_2$ complex,[2] corresponding to two different Pt coordination environments (Figure 4). Both of these resonances are pseudotriplets with an approximate intensity ratio of 1:6:1 (theoretical ratio 1:4:1). The central peak of the triplets, displayed in parts b and c of Figure 4, arises from molecules with one ^{195}Pt ($I = {}^1/_2$; natural abundance = 33.7%) atom and the outer two peaks result from molecules with two ^{195}Pt atoms with coupled nuclear spins. The 6850-Hz value for $^1J(^{195}Pt–^{195}Pt)$ falls at the high end of the range of reported $^1J(^{195}Pt–^{195}Pt)$ values[25] and is larger than those reported for the phosphito- (**12**) and sulfato-bridged (**13**) diplatinum(III) complexes listed in Table V.[26]

The ^{195}Pt chemical shifts in Table V are assigned on the basis of trends established for similar Pt(II) and Pt(III) complexes. The greater the electronegativity of the donor atoms, the more deshielded is the platinum nucleus.[25] The downfield resonance therefore corresponds to the platinum nucleus (Pt(1)) with three nitrogen and two oxygen atoms (N_3O_2) in the coordination sphere while the upfield resonance corresponds to the platinum nucleus (Pt(2)) bonded to four nitrogen atoms and one oxygen atom (N_4O).

Although few comparable $[Pt^{III}]_2$ chemical shifts have been reported, the values for **1** relative to the binuclear Pt(II) precursor[2] are consistent with the assignment of the Pt(III) oxidation state for compound **1** in solution. The change in $\delta(^{195}Pt)$ per change in oxidation state unit has been estimated to be 1250 ppm.[27] Comparison of the chemical shifts of similar Pt(II) and Pt(IV) complexes reveals an extensive deshielding of the nucleus as the oxidation state increases. The Pt(III) nuclei in **1** are deshielded relative to the Pt(II) precursor **2**, with the low-field Pt(II) resonance moving 2180 ppm and the high-field resonance 1382 ppm downfield upon oxidation to Pt(III). The differences between the chemical shifts of **1** and **2** also include contributions from strong metal–metal and metal–axial ligand interactions present only in **1**. Chemical shift measurements for other Pt(III) complexes are required to assess the magnitude of these individual contributions, but the change in oxidation state apparently accounts for much of the difference.

Taken together, the ^{195}Pt NMR results for **1** are consistent with the structure shown in Figure 1 persisting in solution.

Decomposition Studies. Freshly prepared aqueous or DMF solutions of **1** show only two ^{195}Pt resonances, but when they are left to stand for an hour at room temperature, two new resonances appear in the Pt(II) chemical shift region. These peaks correspond to the previously assigned head-to-head binuclear platinum(II) complex **2**.[8] At 5 °C, the decomposition rate of **1** is much slower and no Pt(II) complexes with resonances between 0 and −2900 ppm were observed after 6 h.

When the binuclear Pt(III) complex **1** is reduced to **2**, something must be oxidized. There are three possibilities: disproportionation, intramolecular oxidation of a ligand, and intermolecular oxidation of solvent or some other exogenous molecule. The last seems improbable since the decomposition is extensive in deionized water or in dry distilled DMF.

We have, however, found indirect evidence suggesting that intramolecular oxidation of the axial nitrite ligand has occurred. Addition of sodium tetraphenylborate or phenol to freshly prepared, nitrogen-purged aqueous or DMF solutions of **1** results in the formation of nitrobenzene or nitrophenol, respectively.[28] These organic nitration products may arise from the reaction of the nitronium ion, NO_2^+, the species responsible for aromatic nitrations in concentrated HNO_3/H_2SO_4 mixtures, with the organic substrate.[29] This NO_2^+ species could be produced by reductive elimination from the nitrite-capped $[Pt^{III}]_2$ complex in a two-electron process, which would also yield the $[Pt^{II}]_2$ complex. Since the nitronium ion reacts readily with H_2O giving nitric acid,[30] it would be consumed rapidly in the absence of other substrates.

These reactions provide a rationalization for both the decomposition of **1** to a $[Pt^{II}]_2$ complex and the ability of solutions of **1** to promote aromatic nitration reactions. Electrochemical studies in the analogous *cis*-diammine $[Pt^{II}]_2/[Pt^{III}]_2$ system have shown that these complexes undergo quasi-reversible two-electron redox reactions.[5] Oxidative addition of substrates to binuclear platinum(II) complexes has been observed in this and several similar systems capable of forming metal–metal-bonded $[Pt^{III}]_2$ complexes.[31] The present nitration reaction, however, may be a rare example of reductive elimination involving the $[Pt^{II}]_2/[Pt^{III}]_2$ couple.[32]

Conclusions

Structural, magnetic, and chemical analyses show that a sterically strained $[Pt^{II}]_2$ complex, where two platinum atoms are hindered from close approach by ethylenediamine rings, can be oxidized in nitric acid to give a metal–metal-bonded, nitrite/nitrate-capped binuclear platinum(III) complex. ^{195}Pt NMR studies demonstrate that the binuclear metal–metal-bonded $[Pt^{III}]_2$ framework also exists in freshly prepared aqueous and DMF solutions. The complex, however, is not indefinitely stable in these solutions at room temperature and decomposes in a few hours, yielding the $[Pt^{II}]_2$ precursor complex. Fresh solutions of the $[Pt^{III}]_2$ complex are also capable of nitrating organic substrates. These observations are consistent with reductive elimination of the nitronium ion from the nitrite-capped $[Pt^{III}]_2$ complex in a two-electron process, which produces the $[Pt^{II}]_2$ precursor. The nitronium ion is postulated as the agent responsible for the nitration reactions.

Acknowledgment. This work was supported by PHS Grant CA 34992 awarded by the National Cancer Institute, DHHS. We thank Engelhard Industries for a generous loan of K_2PtCl_4, from which all platinum compounds were synthesized, and A. Jain for experimental assistance.

Registry No. **1**, 100349-93-7; **2**, 100334-01-8; nitrobenzene, 98-95-3;

(25) Pregosin, P. S. *Coord. Chem. Rev.* **1982**, *44*, 247–291.
(26) Appleton, T. G.; Hall, J. R.; Neale, D. W.; Ralph, S. F. *Inorg. Chim. Acta* **1983**, *77*, L149–L151.
(27) Kidd, R. G. In "The Multinuclear Approach to NMR Spectroscopy"; Lambert, J. B.; Riddell, F. G., Eds., D. Reidel: Dordrecht, The Netherlands, 1982; p 445.
(28) We considered an alternative explanation for the nitration of the aromatic substrate. If the nitrite ligand dissociated intact from the $[Pt^{III}]_2$ complex, and nitrous acid formed in reasonable quantity, nitration could proceed through attack of the NO^+ ion on the organic substrate. In the presence of HNO_3 the aromatic NO derivative could be oxidized to the nitro derivative: $ArH + HNO_2 \rightarrow ArNO + H_2O$ and $ArNO + HNO_3 \rightarrow ArNO_2 + HNO_2$. The nitration reaction we observe, however, occurs in neat DMF as well as in neutral aqueous solutions. The reaction in DMF is free of HNO_2 and HNO_3, while the aqueous solutions are free of HNO_3.
(29) Stock, L. M. In "Industrial and Laboratory Nitrations"; Albright, L. F., Hanson, C., Eds.; American Chemical Society: Washington, DC, 1977; ACS Symp. Ser. No. 22, p 48.
(30) Cotton, F. A.; Wilkinson, G. "Advanced Inorganic Chemistry: A Comprehensive Text", 4th ed.; Wiley: New York, 1980; p 431.
(31) (a) Che, C.-M.; Schaefer, W. P.; Gray, H. B.; Dickson, M. K.; Stein, P. B.; Roundhill, D. M. *J. Am. Chem. Soc.* **1982**, *104*, 4253–4257. (b) Che, C.-M.; Herbstein, F. H.; Schaefer, W. F.; Marsh, R. E.; Gray, H. B. *J. Am. Chem. Soc.* **1983**, *105*, 4604–4607. (c) Roundhill, D. M. *J. Am. Chem. Soc.* **1985**, *107*, 4354–4356. (d) See ref 1 for other examples.
(32) See: Hedden, D.; Roundhill, D. M.; Walkinshaw, M. D. *Inorg. Chem.* **1985**, *24*, 3146.
(33) Unpublished results.
(34) Lippert, B.; Schöllhorn, H.; Thewalt, U. *J. Am. Chem. Soc.* **1986**, *108*, 525.

sodium tetraphenylborate, 143-66-8; phenol, 108-95-2; 4-nitrophenol, 100-02-7; platinum, 7440-06-4.

Supplementary Material Available: A listing of atomic thermal parameters for **1** (2 pages). Ordering information is given on any current masthead page. According to policy instituted Jan 1, 1986, the tables of calculated and observed structure factors (12 pages) are being retained in the editorial office for a period of 1 year following the appearance of this work in print. Inquiries for copies of these materials should be directed to the Editor.

Contribution from the Department of Chemistry,
Kinki University, Kowakae, Higashi-Osaka 577, Japan

Cadmium-113 NMR of Cadmium(II) Complexes with Ligands Containing N-Donor Atoms. Dependence of the Chemical Shift upon the Ligand Basicity, Chelate Ring Size, Counteranion, and Cadmium Concentration

Megumu Munakata,* Susumu Kitagawa, and Fujio Yagi

Received June 20, 1985

^{113}Cd NMR studies were carried out on a variety of Cd(II) complexes with N-containing ligands. The ^{113}Cd chemical shifts of Cd complexes are affected by the counteranions and the concentration. However, when no ligands of the Cd complexes were replaced by counteranions and/or solvents, the ^{113}Cd chemical shifts were independent of the anions and the concentration within experimental error. ^{113}Cd nucleus deshielding of the complexes with 4-substituted pyridines (L) and 4,5,7-substituted 1,10-phenanthrolines (biL) increased with increasing pK_a of the ligands, and the pK_a dependence was enhanced with the formation of higher order complexes: $CdL^{2+} < CdL_2^{2+} < CdL_3^{2+} < CdL_4^{2+} < Cd(biL)_3^{2+}$. In the case of $Cd(biL)_3^{2+}$, the increase of 1 pK_a unit gave a downfield shift of 8.8 ppm. This demonstrates that ^{113}Cd NMR is very sensitive to the Cd–ligand bonding. The ^{113}Cd resonance of tris(diamine)cadmium also remarkably moves downfield as the chelate ring size decreases from seven to five members, i.e., $Cd(NH_2(CH_2)_4NH_2)_3^{2+}$ (227 ppm) < $Cd(NH_2(CH_2)_3NH_2)_3^{2+}$ (259 ppm) < $Cd(en)_3^{2+}$ (347 ppm). The same trend was observed in the series of dicarboxylate and dithiolate Cd complexes, with the pronounced sensitivity arising from chelate ring strain. The chemical exchange rates of labile Cd complexes in ethanol solution were successfully reduced by the use of low temperature (−90 °C), and all ^{113}Cd resonances of $Cd(pyridine)_n^{2+}$ (n = 0–4) and $Cd(imidazole)_n^{2+}$ (n = 0–6) were observed in solution and assigned. The ^{113}Cd chemical shifts of the solution NMR spectra agreed well with those of the solid NMR spectra for the cadmium complexes with imidazole and biL.

Introduction

Several physical techniques, most notably EPR, optical spectroscopy, and magnetic susceptibility, have been extremely useful in providing insight into the structures of metal complexes and the coordination environment in metalloenzymes, such as those containing Fe(II,III), Co(III), and Cu(II). However, these methods are not available for diamagnetic metal ions such as Cd^{2+}, Zn^{2+}, Cu^+, and Ag^+, which have d^{10} electronic configurations. The chemistry of these metal ions has become of interest in recent years because of their important characteristics of possessing properties of both transition and nontransition elements.[1] Organocadmium compounds have been widely used for organic synthesis.[2] Cadmium also plays an important role in the metallothioneins, which are widespread in nature,[3] and is often used to obtain the cadmium derivative of metalloenzymes such as LADH,[4] alkaline phosphatase,[5] carbonic anhydrase,[6] and superoxide dismutase.[7]

The ^{113}Cd chemical shift has been demonstrated to be remarkably sensitive to the coordination environment of the metal ion, including the donor atoms, coordination number, geometry, and solvent. The deshielding of $^{113}Cd^{II}$ increases in the order O < N < S, and the range of the observed shifts exceeds 900 ppm.[8-11] The ^{113}Cd NMR technique has therefore become a valuable tool in cadmium chemistry and bioinorganic chemistry. It has been mainly applied to the study of metallothionein[12,13] and a wide variety of metalloenzymes[4-7,12,13] in which the native Zn^{2+}, Cu^{2+}, Mg^{2+}, or Ca^{2+} ions are replaced by $^{113}Cd^{2+}$.

Attempts at detailed correlation of solution NMR spectra with the coordination environment in cadmium(II) compounds of known structure are hampered by the fast chemical exchange of cadmium(II) complexes with ligands and solvents. Two limiting situations should be considered. If the exchange is rapid on the NMR time scale, then a single averaged chemical shift is obtained.

(1) Cotton, F. A.; Wilkinson, G. "Advanced Inorganic Chemistry"; Wiley: New York, 1980; pp 589–616.
(2) Negishi, E. "Organometallics in Organic Synthesis"; Wile New York, 1980; Vol. 1, pp 91–285.
(3) Margoshes, M.; Vallee, B. L. *J. Am. Chem. Soc.* **1957**, *79*, 4813. Kojima, Y.; Berger, C.; Vallee, B. L.; Kagi, J. H. R. *Proc. Natl. Acad. Sci. U.S.A.* **1976**, *73*, 3413. Otvos, J. D.; Armitage, I. M. *Proc. Natl. Acad. Sci. U.S.A.* **1980**, *77*, 7094.
(4) Bobsein, B. R.; Myers, R. J. *J. Biol. Chem.* **1981**, *256*, 5313. Bobsein, B. R.; Myers, R. J. *J. Am. Chem. Soc.* **1980**, *102*, 2454.
(5) Gettins, P.; Coleman, J. E. *J. Biol. Chem.* **1983**, *258*, 396. Otvos, J. D.; Armitage, I. M. *Biochemistry* **1980**, *19*, 4031. Chlebowski, J. F.; Armitage, I. M.; Coleman, J. E. *J. Biol. Chem.* **1977**, *252*, 7053.
(6) Jonsson, N. B.-H.; Tibell, L. A. E.; Evelhoch, J. L.; Bell, S. J.; Sudmeier, J. L. *Proc. Natl. Acad. Sci. U.S.A.* **1980**, *77*, 3269. Uiterkamp, A. J. M. S.; Armitage, I. M.; Coleman, J. E. *J. Biol. Chem.* **1980**, *255*, 3911. Evelhoch, J. L.; Bocian, D. F.; Sudmeier, J. L. *Biochemistry* **1981**, *20*, 4951.
(7) Bailey, D. B.; Ellis, P. D.; Free, J. A. *Biochemistry* **1980**, *19*, 591.
(8) Cardin, A. D.; Ellis, P. D.; Odom, J. D.; Howard, J. W. *J. Am. Chem. Soc.* **1975**, *97*, 1672.
(9) Haberkorn, R. A.; Que, L.; Gillum, W. O.; Holm, R. H.; Liu, C. S.; Lord, R. C. *Inorg. Chem.* **1976**, *15*, 2408.
(10) Jensen, C. F.; Deshmukh, S.; Jakobsen, H. J.; Inners, R. R.; Ellis, P. D. *J. Am. Chem. Soc.* **1981**, *103*, 3659. Rodesiler, P. F.; Amma, E. L. *J. Chem. Soc. Chem. Commun.* **1982**, 182.
(11) Carson, G. K.; Dean, P. A. W.; Stillman, M. J. *Inorg. Chim. Acta* **1981**, *56*, 59.
(12) Otvos, J. D.; Armitage, I. M. "Biochemical Structure Determination by NMR"; Bothner-By, A. A., Glickson, J. D., Sykes, B. D., Eds.; Marcel Dekker: New York, 1982; pp 65–96. Armitage, I. M.; Otvos, J. D. *Biol. Magn. Reson.* **1982**, *4*, 79–144. Armitage, I. M.; Otvos, J. D.; Briggs, R. W.; Boulanger, Y. *Fed. Proc., Fed. Am. Soc. Exp. Biol.* **1982**, *41*, 2974. Boulanger, Y.; Armitage, I. M.; Miklossy, K.-A.; Winge, D. R. *J. Biol. Chem.* **1982**, *257*, 13717. Suzuki, K. T.; Maitani, T. *Experientia* **1978**, *34*, 1449.
(13) Sudmeier, J. L.; Green, D. B. "The Coordination Chemistry of Metalloenzymes"; Bertini, I., Drago, R. S., Luchinat, C., Eds.; D. Reidel: New York, 1983; pp 35–47. Gettings, P.; Coleman, J. E. *Fed. Proc., Fed. Am. Soc. Exp. Biol.* **1982**, *41*, 2966.

0020-1669/86/1325-0964$01.50/0